Proteomic and Lipidomic Analysis of Nanoparticle Corona upon Contact with Lung Surfactant Reveals Differences in Protein, but Not Lipid Composition

Simon Sebastian Raesch,[†,‡] Stefan Tenzer,[§] Wiebke Storck,[§] Alexander Rurainski,[⊥] Dominik Selzer,[⊥] Christian Arnold Ruge,[†] Jesus Perez-Gil,[∥] Ulrich Friedrich Schaefer,[†] and Claus-Michael Lehr*[,†,‡]

[†]Department of Pharmacy, Saarland University, 66123 Saarbruecken, Germany, [‡]HIPS — Helmholtz Institute for Pharmaceutical Research Saarland, Helmholtz Centre for Infection Research, 66123 Saarbruecken, Germany, [§]Institute of Immunology, Mainz University, 55131 Mainz, Germany, [⊥]Scientific Consilience GmbH, Saarland University, 66123 Saarbruecken, Germany, and [∥]Department of Biochemistry and Molecular Biology, Faculty of Biology, Complutense University, 28040 Madrid, Spain

ABSTRACT Pulmonary surfactant (PS) constitutes the first line of host defense in the deep lung. Because of its high content of phospholipids and surfactant specific proteins, the interaction of inhaled nanoparticles (NPs) with the pulmonary surfactant layer is likely to form a corona that is different to the one formed in plasma. Here we present a detailed lipidomic and proteomic analysis of NP corona formation using native porcine surfactant as a model. We analyzed the adsorbed biomolecules in the corona of three NP with different surface properties (PEG-, PLGA-, and Lipid-NP) after incubation with native porcine surfactant. Using label-free shotgun analysis for protein and LC—MS for lipid analysis, we quantitatively determined the corona composition. Our results show a conserved lipid composition in the coronas of all investigated NPs regardless of their surface properties, with only hydrophilic PEG-NPs adsorbing fewer lipids in total. In contrast, the analyzed NP displayed a marked difference in the protein corona, consisting of up to 417 different proteins. Among the proteins showing significant differences between the NP coronas, there was a striking prevalence of molecules with a notoriously high lipid and surface binding, such as, *e.g.*, SP-A, SP-D, DMBT1. Our data indicate that the selective adsorption of proteins mediates the relatively similar lipid pattern in the coronas of different NPs. On the basis of our lipidomic and proteomic analysis, we provide a detailed set of quantitative data on the composition of the surfactant corona formed upon NP inhalation, which is unique and markedly different to the plasma corona.

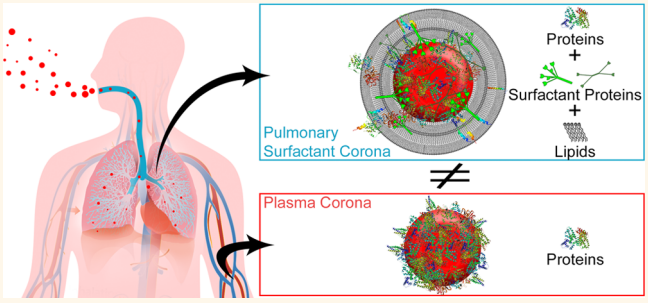

KEYWORDS: bronchoalveolar lining fluid · nanoparticle surface · biological barrier · bionano interface · inhalation · lipid—protein interaction · magnetic separation

The nanobio interface is defined not only by nanoparticle—cell interactions, but also by the interaction of nanoparticles (NPs) with the biological fluid, that NPs encounter upon entry into a biological system. This applies to all nanomaterials, regardless of their intended use, *e.g.*, technical or pharmaceutical, and regardless of the route of exposure/application to the human body.[1,2] According to their definition, so-called "nanomedicines" may range up to several hundred nanometers in size.[3] Solid nanoparticles have been found to interact with a range of proteins in the blood and extracellular fluids,[4,5] attracting an entity of adsorbed molecules referred to as "corona".[6] This corona is composed of a "hard" corona, the strongly bound layer, driven by high affinity toward the surface, and a "soft" corona, a layer of proteins, loosely bound onto the first mentioned, which is characterized by low affinity and high exchange rates with other proteins.[2,7] The hard corona crucially impacts the interaction of NPs with cells, therewith determining directly not only the fate of the NPs,[8—11] but also the properties of the NPs such as its drug release.[9] The in-depth analysis of the NP corona has been enabled by label-free shotgun proteomics.

* Address correspondence to claus-michael.lehr@helmholtz-hzi.de.

Received for review July 8, 2015 and accepted November 16, 2015.

Published online 10.1021/acsnano.5b04215

Several studies have addressed the adsorption behavior of single proteins and complex fluids with various nanomaterials, allowing meanwhile a first physical description of the interaction mode and kinetics.[11,12] However, most studies focused exclusively on the interaction of NP with plasma. Limited attention has been paid to other relevant biological fluids. Notably, the respiratory tract is the most likely path for NPs to enter the body. In contrast to larger particles, the small size of NPs enables them to reach the deep lung. Therefore, both future pulmonary applications of NPs as drug delivery vehicles and nanotoxicological considerations, *e.g.*, addressing the inhalation of respirable dust, crucially require data addressing the fate of NPs after deposition in the deep lung.[13,14]

The air-blood barrier is built by alveolar epithelial cells type-1 (AT-I), which can be as thin as 25 nm and are differentiated from alveolar epithelial type-2 cells (AT-II). The alveoli and its cells, although very thin, withstand enormous pressure and size changes during the breathing cycle. To prevent the alveolar sacs from collapsing and conglutination at the end of exhalation, the surface tension at the air-cell interface is lowered by a thin liquid layer which is enriched by lipids and proteins, the "pulmonary surfactant" (PS) that is secreted by AT-II cells. PS displays an unique composition, which reduces the surface tension to values lower than 2 mN/m and maintains such low tensions during the moderately long periods of time required for the lungs to be emptied. The mechanisms of this effect are yet to be completely understood, but are a result of the synergistic interaction between the prevailing lipids and characteristic proteins. Until now, four pulmonary surfactant associated proteins (SP-A, -B, -C, and -D) have been identified in PS, which can be divided in two groups. The two highly hydrophobic SP-B and SP-C modulate and dynamize the behavior of the lipid layers. Together with the saturated amphiphilic surface active dipalmitoylphosphatidylcholine (DPPC), the major lipid constituent of PS, and a whole range of other (mainly phospho-) lipids, the phase transition temperature of the PS layer is matched to around the physiological temperature of 37 °C. Between 25−41 °C PS assembles into an impressive set of highly organized lamellar structures, exhibiting a conspicuous coexistence of ordered and disordered phases.[15−17]

The two hydrophilic proteins, *i.e.*, SP-A and SP-D, belong to the collectin family and are connected to the innate immune response.[18] At least SP-A is also associated with the lipid membranes and takes part in the organization of the lipid−protein complexes. Although SP make up for only about 5% in total, they are essential for the PS to fulfill its physiological function. Moreover, only 5% of the PS are composed of other proteins which differ from the plasma proteome likewise.[17,19]

This peculiar composition of the PS layer likely leads to the formation of a NP corona which is substantially different from the NP corona formed in plasma. While we have previously investigated the composition of a plasma corona on NPs in great detail[5,20] only little is known about the interaction of airborne NPs with the highly complex PS fluid. We showed recently, that SP-A adsorption can have an influence on the uptake of NPs into alveolar macrophages, but this effect was equalized in the presence of lipids.[21] Kapralov *et al.* found an enhanced macrophage uptake of single-walled carbon nanotubes (SWCNT) in the presence of SP-D, which was further increased in the presence of phospholipids (PL).[22] Furthermore, phosphatidylserine coated SWCNT were preferably taken up by macrophages.[23] Notably, both phospholipids and proteins adsorb to carbon nanotubes after inhalation,[22] and in return, SWCNT also alter the lipidomic profile of the lung tissue.[24] Sachan *et al.* performed a series of atomic force microscopy experiments, which showed that hydrophobic NPs are interacting strongly with a model surfactant layer composed of DPPC, DPPG and SP-C, adsorbing at least two layers of phospholipids.[25,26]

In the present study, we comprehensively analyzed the corona which is formed around NPs after contact with the PS, which is obviously the first body fluid encountered after deposition in the deep lung. As the PS contains proteins as well as lipids, we have quantitatively addressed both components using label-free shotgun proteomics in combination with LC−MS lipidomic analysis to comprehensively characterize the complex composition of the PS corona. Using three types of NPs, differing in their surface properties and hydrophobicity, our data enabled the first complete proteomic and lipidomic analysis of the NP corona as formed after incubation with native pulmonary surfactant.

RESULTS AND DISCUSSION

How to Probe the Pulmonary Surfactant Corona? The plasma protein NP-corona is likely one of the most intensively investigated topics in nanobiosciences,[1] which is also facilitated by the fact that human plasma is quite easily accessible. In contrast, PS is typically obtained by bronchoalveolar lavage (BAL) and the availability of BAL fluid is rather limited. BAL maybe performed on healthy volunteers by bronchoscopy, which is a rather invasive procedure and produces only small amounts of BAL fluid, insufficient for thoroughly studying nanobio interactions.

Experiments in small animals such as mice are of high importance for toxicity evaluation,[27,28] in consideration of the fact that the true mode of exposure can be assessed realistically only *in vivo*. For the sake of animal welfare, however, *in vivo* or *ex vivo* experiments in small animals are not desirable as a standard screening procedure of the nanomaterial corona in PS.

For medical purposes, only few different animal-derived surrogates of PS are commercially available.

TABLE 1. Top 20 Most Abundant Proteins Found in pPS and Crude Plasma[20] as Determined by Label-Free Shotgun Proteomics[a]

native surfactant			crude plasma (taken from[20])		
proteins	rel. abundance [%]		proteins	rel. abundance [%]	
pulmonary surfactant-associated protein A	10.19	±*0.39*	**serum albumin**	**23.15**	±**4.80**
serum albumin	**5.77**	±**0.18**	alpha-2-macroglobulin	11.04	±0.98
sodium-dependent phosphate transport protein 2B	2.31	±0.11	**complement C3**	**8.80**	±**0.39**
tubulin alpha-4A chain	2.27	±0.04	Ig gamma-1 chain C region	7.70	±0.77
fibronectin	2.23	±0.07	**serotransferrin**	**5.01**	±**0.24**
myosin-9	2.09	±0.11	alpha-1-antitrypsin	4.60	±0.86
deleted in malignant brain tumors 1 protein	1.99	±0.11	haptoglobin	3.51	±0.36
complement C5	1.85	±0.09	apolipoprotein A-I	3.26	±0.60
actin, cytoplasmic 1	1.80	±0.10	Ig kappa chain C region	2.42	±0.16
complement C3	**1.68**	±**0.19**	Ig gamma-2 chain C region	2.20	±0.25
pulmonary surfactant-associated protein B	1.39	±*0.11*	complement C4-A	2.09	±0.14
Ig alpha-1 chain C region	**1.28**	±**0.08**	**Ig alpha-1 chain C region**	**2.07**	±**0.31**
hemoglobin subunit beta	1.23	±0.01	Ig gamma-4 chain C region	2.05	±0.06
l-xylulose reductase	1.14	±0.06	hemopexin	1.79	±0.13
tubulin beta-4B chain	1.02	±0.07	ceruloplasmin	1.35	±0.12
tubulin alpha-1A chain	1.02	±0.07	Ig lambda chain C regions	0.91	±0.04
calcium-activated chloride channel regulator 1	0.96	±0.04	alpha-1-antichymotrypsin	0.89	±0.05
polymeric immunoglobulin receptor	0.94	±0.03	interalpha-trypsin inhibitor heavy chain H2	0.88	±0.07
AP-2 complex subunit beta	0.94	±0.08	complement factor H	0.81	±0.07
serotransferrin	**0.92**	±**0.03**	Ig mu chain C region	0.80	±0.08

[a] Although there are serum proteins among the most abundant proteins in the pPS preparation, most proteins do not occur in plasma. The most abundant protein in pPS is the collectin SP-A, which is responsible for lipid organization and part of innate host defense. Additionally, the highly hydrophobic SP-B is present among the top 20 proteins. Proteins occurring in both lists are marked bold.

These preparations are basically organic extractions from minced or lavaged animal lungs such as Survanta (AbbVie, bovine minced lung), Alveofact (Lyomark, bovine lavaged lung), or Curosurf (Chiesi, porcine minced lung). All preparations have in common that proteins are depleted to prevent immunogenic reactions. The hydrophobic SP-B and SP-C, however, have a reduced immunogenicity and are essential for the surface lowering effects of the PS, and therefore remain in the extracts.[29] Recently Pohlmann *et al.* introduced an inhaler with an artificial phospholipid mixture with a recombinant SP-C.[30] These preparations mimic the physical properties of the native surfactant, the real corona of NPs, nevertheless, remains not accessible. Furthermore, Beck-Broichsitter *et al.* were able to show that the physiological function of a simple artificial surfactant lipid mixture is inhibited after contact with polymeric NPs.[31] This effect was diminished with increasing complexity of the preparation, with a native PS preparation being nearly unaffected. Looking for an adequate surrogate of human PS, we have chosen a native PS preparation obtained from pigs, which has been demonstrated to feature all essential components and physiological functions.[19,32−34] Porcine pulmonary surfactant (pPS) can be obtained from BAL of slaughtered pigs' lungs, a scheme of the preparation process is shown in Figure S1 in the Supporting Information.

Having selected an adequate model, further difficulties become obvious. Unlike with proteins alone, the lipid-based membranes of PS make the investigation of the NP corona challenging. Essential for its physiological function, the PS structures show high fluidity in the lungs. This effect is facilitated by its phase transition temperature. At 37 °C, PS lipid layers are at the edge of a critical structural transition, resulting in a very dynamic behavior of the exposed surfaces and the possibility for inhaled particles to interact with the lipids and the proteins which are strongly associated with the former. At lower temperatures, NPs will interact with accessible molecules only in the relatively more fluid regions and this will not result in the formation of a realistic corona, regarding the high evidence for lipid−protein interactions.[15,35−37] The influence of temperature on the colloidal behavior of pPS as observed by dynamic light scattering at 4 and 37 °C is shown in Supplemental Figure S2. At 4 °C (Figure S2A), pPS presents itself as stable, liposome-like vesicles, whereas at 37 °C (Figure S2B), there are no defined peaks visible in the DLS measurements. The peaks are heavily scattering, as the lipid layers perpetually interact with each other, changing size within seconds and offering different epitopes toward intruding NPs.

The structural dynamics and the self-organization of large membrane complexes result in sedimentation of the surfactant in *in vitro* experiments. We compared three different methods to separate the NPs together with their corona from the incubation fluid (Supplemental Figure S3). Unfortunately, simple

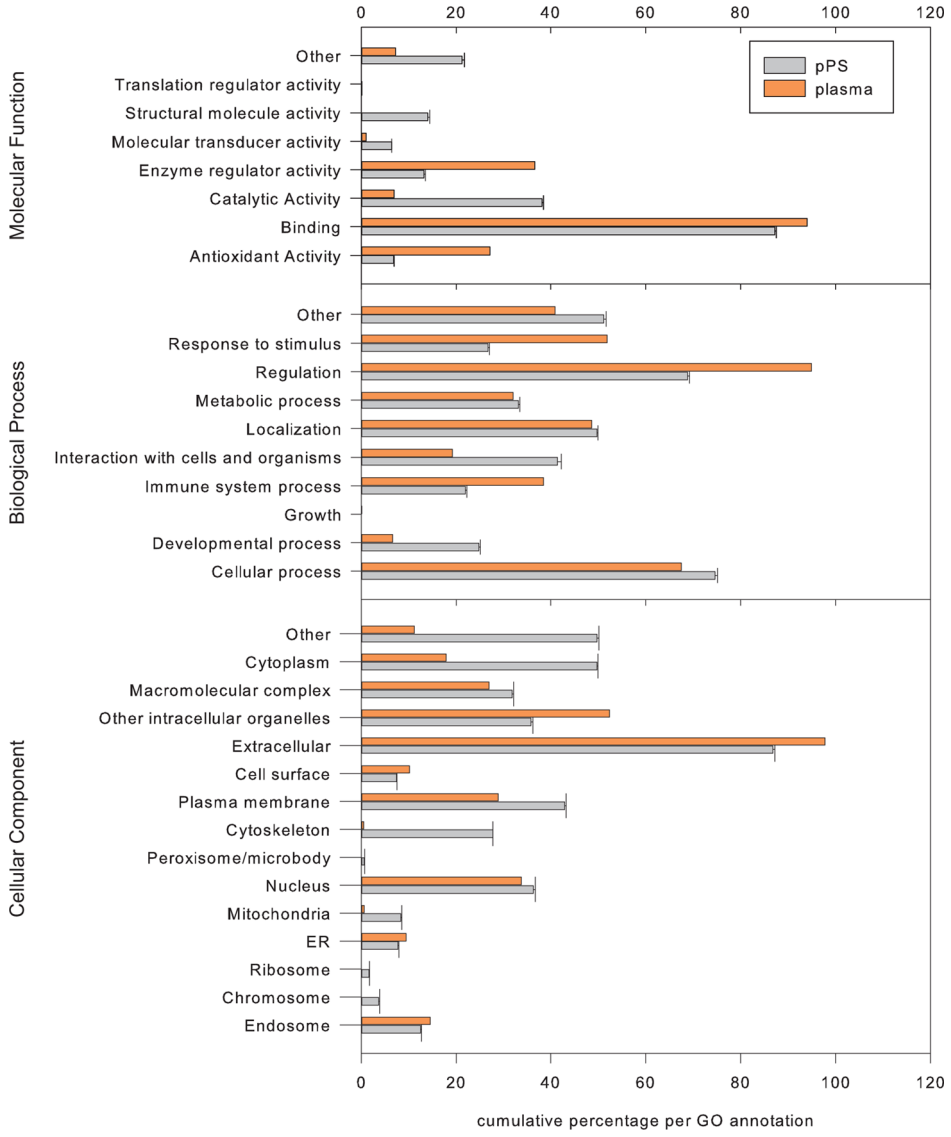

Figure 1. Comparison of the proteins found in crude plasma[20] and native Surfactant (pPS) by means of their cumulated relative amount per gene ontology annotations (GO slim, STRAP 1.5). Although GO slim terms generalize the annotations, a different distribution of the composition is obvious. Predominantly, catalytic activity, interaction with cells and organisms, and plasma membrane are increased in pPS.

centrifugation as proposed for plasma by Monopoli *et al.*[38] turned out to be not feasible in PS as the vesicle-like lipid−protein complexes of PS are also prone to sedimentation (Figure S3A). Tenzer *et al.*[39] showed that the separation of NPs from plasma can rapidly be achieved by centrifugation through a cushion of higher density. In our experiments, however, the surfactant alone still showed sedimentation, although density was adequately adjusted (Figure S3B). While in another study Monopoli *et al.*[40] found no major impact of different separation methods on the observed corona in plasma, we found for pPS that only magnetic separation (Figure S3C) resulted in clear separation of the NPs from the incubation fluid. Because magnetic separation avoids the influence of sedimentation and lesser forces are applied, a clear separation from the background was achieved, as indicated by a negligible pellet in the blank control (compare first column of Figure S3A−C).

In order to be able to use magnetic separation, we chose magnetite loaded NPs which are commercially available with rather different surface chemistry: NPs with phosphatidylcholine-(fluidmag-lipid; chemicell GmbH, Germany; further referred to as "Lipid-NP") and PEG5000-coating (nanomag-D PEG5000; micromod Partikeltechnologie GmbH, Germany; further referred to as "PEG-NP"). Furthermore, we decided to include also magnetite-loaded NPs made of poly(lactic-*co*-glycolic acid) (PLGA-NP), a well-accepted pharmaceutical excipient, potentially also to be used in future inhalation nanopharmaceuticals.

Proteomic and Lipidomic Profile of Native Porcine Pulmonary Surfactant Preparation. By comparing the top 20 most abundant proteins in crude plasma and pPS (Table 1),

TABLE 2. Lipid Composition of Crude Native Pulmonary Surfactant from Porcine Source As Determined by Normal Phase LC–MS and Enzymatic Assay (Cholesterol) after Solid–Liquid Extraction[a]

lipid	GPChol	SM	GPGlyc	GPEth	GPIno	GPSer	chol	total
Total number of lipids quantified	94	3	41	35	58	17	1	249
wt % of total lipids	67.1 ± 3.8	0.2 ± 0.1	5.9 ± 1.2	2.0 ± 0.3	16.8 ± 1.9	0.1 ± 0.0	7.9 ± 1.0	100
% thereof Lyso-PL	3.5 ± 0.4	0	4.8 ± 0.6	0.5 ± 0.0	0	0	–	2.6
% thereof saturated	71.3 ± 4.2	72.0 ± 1.8	27.2 ± 2.1	0.4 ± 0.0	7.4 ± 0.6	0.0	–	48.0
most abundant species	32:0 (DPPC) 54.7 ± 5.0	34:1 63.2 ± 2.3	34:1 36.4 ± 1.1	36:2 17.5 ± 0.2	34:1 14.1 ± 0.6	36:1 71.0 ± 7.8		
	30:0 13.3 ± 2.4	32:2 28.0 ± 1.8	32:0 18.2 ± 2.2	34:1 15.3 ± 0.2	36:2 5.8 ± 0.2	36:2 7.2 ± 4.3		
	34:1 13.3 ± 2.3	32:1 8.8 ± 0.9	34:2 8.7 ± 0.4	34:2 13.7 ± 0.2	36:1 5.2 ± 0.4	38:4 7.0 ± 5.1		
	32:1 10.5 ± 1.5		32:1 8.6 ± 0.3	36:3 13.6 ± 0.3	others 74.9	others 14.8		
	others 8.2		others 28.0	others 39.8				

[a] As previously described, GPChol was the most abundant class, DPPC the most abundant lipid. (GPChol: phosphatidylcholine, SM: sphingomyelin, GPGlyc: phosphatidylglycerol, GPEth: phosphatidylethaolamine, GPIno: phosphatidylinositol, GPSer: phosphatidylserine, Chol: cholesterol).

Figure 2. Absolute amount of adsorbed lipids (= GPChol, GPEth, GPGlyc, GPSer, GPIno, Cholesterol) per m^2 surface area of PLGA-, PEG-, Lipid-NPs as measured by normal phase LC–MS after 1 h incubation at 37 °C with pPS and repeated magnetic separation. Lipid-NPs adsorb as expected more lipids than PLGA-, and PEGNPs, although a direct binding of phospholipids with PEG-NPs was not anticipated.

the differences between these two biological fluids become obvious. Only four proteins can be found in both lists, while the most abundant protein in pPS, SP-A, as well as the hydrophobic SP-B, which are both essential for PS organization, did not appear in crude plasma at all. The presence of blood proteins such as serum albumin and serotransferrin can be explained by the fact that already smallest, nonvisible ruptures during BAL may result in a contamination of alveolar lining fluid with plasma proteins. Until now it was thought that a highly concentrated surfactant preparation, such as the one described here, would only consist of the lipid membranes and proteins which are directly associated with the former. Our proteomic approach showed the presence of SP-D in the preparation, which was previously thought to be lost during purification. The hydrophilic collectin is connected to innate host defense, but the association with lipid vesicles was found to be weaker than that of SP-A.[18] As the label-free shotgun proteomics workflow applied in this study requires the measured proteins to have a minimum size as well as cleavage sites for digesting enzymes, the small and highly hydrophobic surfactant associated protein C (4.2 kDa) was unfortunately not detectable by our approach.

The depiction of the found proteins by means of their biological annotations (GO slim by STRAP 1.5, see Figure 1) show a clear prevalence of "binding" (87%) and "catalytic activity" (38%) for the molecular function domain. A majority (86%) can be found in the extracellular space and can be assigned to several biological processes (Figure 1). Although the gene ontology terms of the proteins are generalized vigorously by the GO slim subset, the comparison of pPS with crude plasma shows differences in the two protein sets: in the

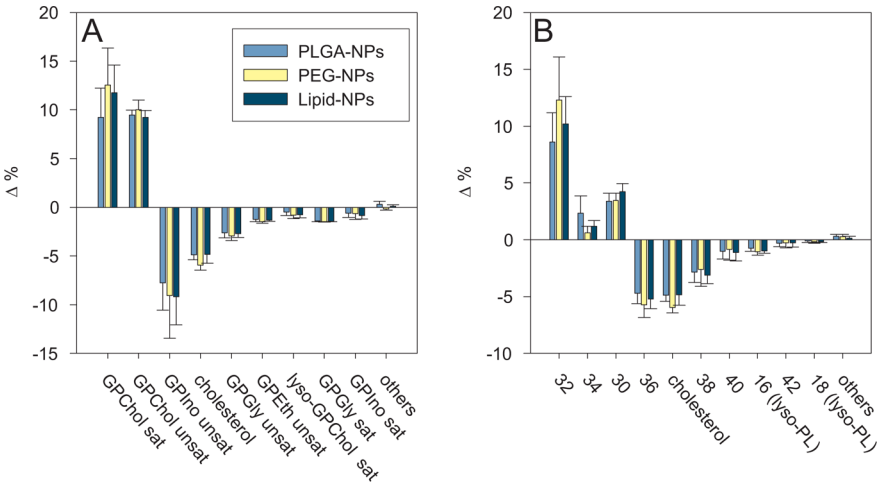

Figure 3. Relative lipid distribution in the pPS corona of PLGA-, PEG-, and Lipid-NPs after 1 h incubation at 37 °C and repeated magnetic separation, in comparison to crude pPS by lipid class (A) and overall chain length of phospholipids (B). The lipid corona of the NPs differs from the composition found in pPS, but it is comparable among the particles. GPIno and Cholesterol are decreased in the corona, while GPChol is increased. This is accompanied by an increased adsorption of lower chain length (B) phospholipids in the NPcorona (sat: saturated PL, unsat: unsaturated PL).

molecular function tree, structural activity and catalytic activity are increased, while in plasma, more proteins show antioxidant and enzyme regulator activity. Interaction with cells and organisms is increased in the pPS proteome, implying the interaction with cells such as macrophages as well as intruding pathogens. More proteins in pPS are connected with the plasma membrane and the cytoplasm.

Additionally to the divergent protein composition, PS is mainly composed of lipids. Thus, we determined the lipid composition to a high level by LC−MS analysis. An overview of the found lipids is presented in Table 2. As reported before, the main constituent of PS was the saturated glycerophosphocholine (GPChol) DPPC. While cholesterol was ignored for a long time, it is now recognized as an important constituent, which influences the fluidity of PS membranes.[41] We determined a cholesterol concentration of 7.9 wt % in the preparation, meeting earlier reported values.[41] Glycerophosphoinositol (GPIno) was the second most abundant lipid class, adding up to 16.8 wt %, similar to the findings of Blanco *et al.*[32] Beside glycerophosphoglycerols (GPGlyc) (5.9 wt %) and glycerophosphoethanolamines (GPEth) (2.0 wt %), we also found traces of glycerophosphoserine (GPSer) and sphingomyelin (SM) (0.1 and 0.2 wt % respectively). Although the lipid mixture is very complex, the majority of lipids were only found in traces, while just a few lipids add up to a large extent. Our approach is to date the most detailed lipid analysis of a porcine pPS preparation which confirmed and extended the values found in the literature.[32,42] The protein−lipid ratio was found to be about 1:10 as described before with a protein and lipid concentration in the crude pPS preparation of ∼3 mg/mL and ∼32 mg/mL respectively. These data indicate that the interaction of NPs with PS, and in particular the corona formed upon contact with this peculiar body fluid, is clearly different to the one formed after interaction of NPs with plasma.

The Lipid Corona of Nanoparticles in Pulmonary Surfactant. After 1 h incubation of NPs with pPS at 37 °C and repeated magnetic separation, the lipids were extracted as described in the Materials and Methods section and analyzed by normal phase LC−MS. The comparison of the absolute lipid amount which attaches to the NP surface (Figure 2) reveals that the NPs adsorb significantly different amounts of lipids per m^2 surface area in the order PEG- (0.12 mg/m^2), PLGA- (0.38 mg/m^2) Lipid-NPs (0.61 mg/m^2). This binding affinity mirrors the hydrophobicity of the NPs, albeit an attraction of lipids by the hydrophilic PEG-NPs was not to be expected in the first place. Zuo *et al.* demonstrated by molecular dynamics simulation, that the interaction of a hydrophilic NP with a DPPC/POPG/SP-C/SP-B layer was diminished and therewith the localization in the layer shortened, in comparison to a lipophilic NP.[43]

The relative distribution of lipids in the corona of all three particles (Figure 3) differed from the relative amount of lipids found in crude pPS. We observed significant changes in concentration of GPChol which was increased on NPs (in average by 11.2% and 9.6%, saturated and unsaturated respectively); all other classes showed decreased concentrations (Figure 3A). Simultaneously, PL with total chain lengths of 32 and 30 carbons (corresponding to the length of both acyl chains), which is less than the average chain length, preferably bound to the NPs. This applied to all NP coronas, notwithstanding their surface properties (Figure 3B). The assumption, that the higher fluidity of the short-chain PL comes along with their location in the most dynamic regions of PS structures in which

TABLE 3. Top 25 Proteins Found in the Corona of PLGA-, PEG- and Lipid-NPs, Sorted by Abundance[a]

PLGA-NPs			PEG-NPs			lipid-NPs		
protein	[%]	STD	protein	[%]	STD	protein	[%]	STD
Tubulin alpha-4A chain	9.29	±0.56	Tubulin alpha-4A chain	9.25	±0.30	Tubulin alpha-4A chain	8.90	±0.55
Actin, cytoplasmic 1	8.04	±0.29	Actin, cytoplasmic 1	8.59	±0.33	Actin, cytoplasmic 1	7.32	±0.25
Hemoglobin subunit beta	6.03	±0.28	Hemoglobin subunit beta	7.31	±0.48	Hemoglobin subunit beta	6.01	±0.20
L-xylulose reductase	5.28	±0.31	L-xylulose reductase	5.91	±0.21	L-xylulose reductase	5.87	±0.31
Tubulin beta-4B chain	3.68	±0.30	Tubulin beta-4B chain	3.74	±0.30	Myosin-9	4.03	±0.24
Tubulin alpha-1A chain	3.59	±0.19	Tubulin alpha-1A chain	3.48	±0.15	Tubulin beta-4B chain	3.84	±0.16
Deleted in malignant brain tumors 1 protein	3.25	*±0.34*	Tubulin beta chain	3.21	±0.30	**Pulmonary surfactant-associated protein A**	**3.73**	**±0.57**
Tubulin beta chain	3.23	±0.21	Myosin-9	2.85	±0.28	*Deleted in malignant brain tumors 1 protein*	3.68	*±0.27*
Pulmonary surfactant-associated protein A	**2.79**	**±0.55**	Fibronectin	2.50	±0.17	Tubulin alpha-1A chain	3.11	±0.14
Myosin-9	2.28	±0.11	Glyceraldehyde-3-phosphate dehydrogenase	2.29	±0.11	Tubulin beta chain	3.09	±0.42
BPI fold-containing family B member 1	2.27	*±0.14*	*Deleted in malignant brain tumors 1 protein*	2.25	*±0.41*	Fibronectin	2.56	±0.17
Fibronectin	2.24	±0.23	Elongation factor 1-alpha 1	1.98	±0.11	*BPI fold-containing family B member 1*	2.01	*±0.15*
Serum albumin	2.03	±0.12	*BPI fold-containing family B member 1*	1.81	*±0.14*	Serum albumin	1.78	±0.15
Glyceraldehyde-3-phosphate dehydrogenase	1.96	±0.14	Serum albumin	1.69	±0.07	Glyceraldehyde-3-phosphate dehydrogenase	1.66	±0.05
Elongation factor 1-alpha 1	1.73	±0.08	**Pulmonary surfactant-associated protein D**	**1.18**	**±0.12**	Elongation factor 1-alpha 1	1.60	±0.08
ADP-ribosylation factor 1	0.98	±0.06	**Pulmonary surfactant-associated protein A**	**1.03**	**±0.14**	Calcium-activated chloride channel regulator 1	0.81	±0.04
Tubulin beta-2B chain	0.83	±0.08	ADP-ribosylation factor 1	0.98	±0.04	ADP-ribosylation factor 1	0.80	±0.04
Retinal dehydrogenase 1	0.83	±0.08	EH domain-containing protein 2	0.92	±0.05	Fatty acid synthase	0.79	±0.04
Complement C5	0.83	*±0.20*	Calcium-activated chloride channel regulator 1	0.90	±0.11	Tubulin beta-2B chain	0.78	±0.10
Calcium-activated chloride channel regulator 1	0.79	±0.06	T-complex protein 1 subunit beta	0.86	±0.07	EH domain-containing protein 2	0.75	±0.05
EH domain-containing protein 2	0.76	±0.04	Pyruvate kinase PKM	0.81	±0.05	*Complement C5*	0.71	*±0.20*
Fatty acid synthase	0.69	±0.03	Retinal dehydrogenase 1	0.81	±0.03	Retinal dehydrogenase 1	0.67	±0.02
Protein-glutamine gamma-glutamyltransferase 2	0.65	±0.03	Fatty acid synthase	0.78	±0.17	Myosin-14	0.67	±0.03
Complement C3	0.64	*±0.10*	*Complement C3*	0.70	*±0.03*	Protein-glutamine gamma-glutamyltransferase 2	0.66	±0.03
Pyruvate kinase PKM	0.63	±0.04	Protein-glutamine gamma-glutamyltransferase 2	0.70	±0.06	Myosin-7B	0.65	±0.45
Total number of proteins identified: 413			**Total number of proteins identified: 376**			**Total number of proteins identified: 417**		

[a] Surfactant associated proteins in bold, other immune response-related proteins in italics. A complete list of identified proteins can be found in the Supporting Information.

their exposure and interaction with surfaces is facilitated, remained speculative.

We observed only minor changes in the lipid corona among the nanoparticles. The comparison of the relative lipid composition in the corona of PLGA- and Lipid-NPs revealed no significant changes, indicating a highly similar lipid corona. In comparison with the PEG-NPs, cholesterol was slightly increased in the corona of PLGA- and Lipid-NPs (both by 1.1%, see Supporting Information, Table S1), while GPIno(34:1) was increased by 1.3% on PLGA-NPs; the other changes were less than 0.1% and not regarded as relevant. The top 10 most abundant lipid species (Supporting Information, Table S1) further revealed that about 90% of the corona of NPs consists of only ten lipids and their analysis might be regarded as sufficiently accurate for future interaction studies. Although PEG- and Lipid-coated NPs can be regarded as oppositely functionalized, the difference in the lipid corona composition was only minimal. Therefore, our data suggested, that the hypothesis that nanoparticles preferably adsorb some lipids over others is questionable, although future studies should address NP surface charge as a factor possibly influencing lipid adsorption. However, the number of lipid bilayers forming around NPs is unknown and so is the amount of lipids which is in direct contact with the NP surface. Our lipidomic data indicated that the multilayered composition of the pPS may mask the surface of the respective NPs.

We therefore concluded that the lipid binding on the PEG-NP surface, although weaker than on the hydrophobic particles, is likely mediated by proteins. To prove this hypothesis, NPs were incubated with the organic PS extract Alveofact (containing only the surfactant lipid fraction and the hydrophobic Surfactant associated proteins B and C) under the same conditions and using the same amount of lipids per NP (~20 μg phospholipids/μg NPs). As revealed by thin layer chromatography (Supporting Information, Figure S4A, only GPChol as most distinctive band shown), lipids were only adsorbed to the Lipid-NPs, but—in contrast to incubation with complete pPS—no longer to the PLGA-NPs or PEG-NPs. The adsorption behavior of lipids could not be enhanced by addition of serum proteins in an equal amount as the protein concentration in our pPS preparation (Figure S4B). Presuming an identical phase behavior of the protein-depleted Alveofact vesicles and pPS, the binding of PEG- and PLGA-NPs must be influenced by the capabilities to bind lipid-attracting proteins.

The Protein Corona of Nanoparticles in Pulmonary Surfactant. Because of the high lipid content of the samples, the absolute amount of proteins that adsorbed to the surface of NPs could only be estimated. Both the estimation based on the shotgun proteomics and the analysis by bicinchoninic acid assay indicated that the ratio of protein to lipid did not change and remained

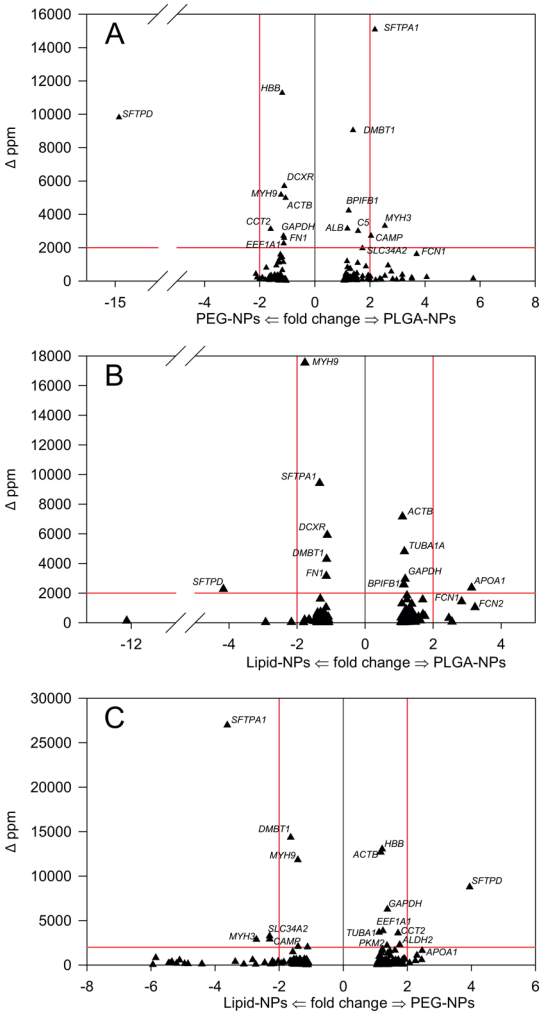

Figure 4. (A–C) Direct comparison of the relative composition of the protein corona on the three different NPs against each other by terms of fold change and ppm change. (The proteins are identified by their gene name: SFTPA1 – Pulmonary surfactant-associated protein A, HBB – Hemoglobin subunit beta, DMBT1 – Deleted in malignant brain tumors 1 protein, SFTPD – Pulmonary surfactant-associated protein D, MYH9 – Myosin-9, MYH3 – Myosin-3, ACTB – Actin, cytoplasmic 1, DCXR – L-xylulose reductase, GAPDH – Glyceraldehyde-3-phosphate dehydrogenase, BPIFP1 – BPI fold-containing family B member 1, FCN-1 – Ficolin-1, FCN2 – Ficolin-2, FN1 – Fibronectin, TUBA1A – Tubulin alpha-1A chain, ALB – Albumin, C5 – Complement C5, CAMP – Cathelicidin antimicrobial peptide, CCT2 – T-complex protein 1 subunit beta, EEF1A1 – Elongation factor 1-alpha 1, SLC34A2 – Sodium-dependent phosphate transport protein 2B, APOA1 – Apolipoprotein A-I, ALDH2 – Aldehyde dehydrogenase 2, PKM2 – Pyruvate kinase PKM). Only proteins with a significant change ($p < 0.05$) are shown. Red vertical lines indicate a fold change threshold of ±2, red horizontal line an arbitrary threshold of 2000 ppm.

approximately 1:10 on all particles (data not shown) in agreement with former results by Kapralov *et al.*[22]

At the first sight of the protein corona composition, the adsorption behavior appeared comparable with the lipid corona: The most abundant proteins on the NPs (Table 3) did not reflect the concentration in the supply of native surfactant (Table 1). By comparing the distributions of proteins in the corona of NPs by means

TABLE 4. Adsorption Pattern of Proteins above the Threshold of 2000 Δppm and ±2 Fold Change and Other Selected Proteins, Known to Be Part of Host Defense and/or Capable of Binding Lipids That Are Varying among NPs Sorted by Their Affinity Towards the Three NPs[a]

	protein		nanopartides			abundance [ppm]	
	name (gene symbol)	relevant annotations	PLGA	PEG	lipid	pPS	plasma (from[20])
fold change >2/<−2 AND Δppm >2000	Surfactant Protein A (SFTPA1)	PL- binding and organization, carbohydrate binding, host defense	++	+	+++	101882.8	Not detected
	Surfactant Protein D (SFTPD)	Carbohydrate binding, interaction with PL, host defense	+	+++	++	5119.0	Not detected
	Cathelicidin antimicrobial peptide (CAMP)	Binds to bacteria, antibacterial, exosome associated	++	+	+++	1736.3	Not detected
	Myosin-3 (MYH3)	–	+++	+	++	6689.6	Not detected
	Apolipoprotein A-I (APOA1)	PL and Chol binding	+++	++	+	3805.1	32563
	Sodium-dependent phosphate transport protein 2B (SLC34A2)	Involved in surfactant synthesis, membrane-associated	+++[b]	+	+++[b]	23086.1	Not detected
fold change >2/<−2 OR Δppm >2000	Deleted in malignant brain tumors 1 protein (DMBT1)	Interacts with SP-D, binds to bacteria, receptor activity, membrane associated	++	+	+++	19865.7	Not detected
	BPI fold-containing family B member 1 (BPIFB1)	Binds LPS, modulates cell response, binds PL	++	+	+++	8788.5	Not detected
	Ficolin 1/2 (FCN1, FCN2)	Binds pathogen-associated molecular patterns, membrane associated, excreted by macrophages	+++	+	++	2709.9/1426.7	Not detected

[a] +++ = highest relative corona concentration, + = lowest relative concentration. [b] No statistical difference.

of molecular weight, isoelectric point and overall hydrophobicity (GRAVY score), no adsorption pattern, based on these properties, became visible (Supporting Information, Figure S5). There were however differences among the NPs regarding individual proteins. On all three NPs, the four most abundant proteins in all three NPs were tubulin alpha-4a-chain, actin cytoplasmic 1, hemoglobin subunit beta and L-Xylose reductase, with other tubulins within the top 25. These peptides do not appear to be directly linked to PS functions, and may constitute contaminations of the pPS with cytoplasmic proteins which were introduced during BAL. Hemoglobin has been recently described as synthetized and secreted by type II pneumocytes together with pulmonary surfactant complexes,[44,45] and modified variants of the hemoglobin beta chain have been identified as strongly associated with surfactant membranes.[46] The ubiquitous actin, myosin and tubulin present in microtubules, have been found to play a role in surfactant secretion.[47] Tubulin was also found to strongly interact with GPChol vesicles.[48] L-xylulose reductase is suspected to be membrane-bound and might interact with GPIno.

Next, we performed pairwise comparisons of proteins adsorbed to the different NPs based on significant differences in fold change (Figure 4), which is a parameter for binding affinity, and the overall concentration change (Δppm). Interestingly, the proteins which stand out by either Δppm, fold change or both, are largely connected to the immune system (Table 4 summarizes the most interesting proteins). We expected proteins to differ in their concentration among the NPs coronas according to their affinity toward the pristine nanomaterial. With an applied threshold of ±2 fold change and 2000 Δppm, all but 6 proteins are excluded: SP-A (gene name: SFTPA1), SP-D (SFTPD), Cathelicidin antimicrobial peptide (CAMP), Myosin-3 (MYH3), Apolipoprotein A-I (APOA1), and Sodium-dependent phosphate transport protein 2B (SLC34A2). The collectin SP-A was present in all three coronas, although decreased in comparison to the pPS reservoir, but with increasing concentrations in the order PEG- < PLGA- < Lipid-NPs. It is known that SP-A readily interacts with phospholipids and can therefore directly bind to Lipid-NPs, as well as the still hydrophobic PLGA-NPs. The mode of binding, by either a targeted binding by its carbohydrate recognition domain or unspecific with its hydrophobic tail, remains to be clarified. Binding of SP-A to the PLGA-NP surface could already be an explanation for a consecutive lipid binding. The concentration of SP-D in PLGA- and Lipid-NPs was rather low (714 and 2977 ppm respectively); in the corona of PEG-NPs, however, the collectin was increased to 11757 ppm, and reached with a fold change of 14.7 compared to PLGA-NPs and 4.0 to Lipid-NPs the top 20 proteins with a higher concentration than SP-A. SP-D is also known to interact

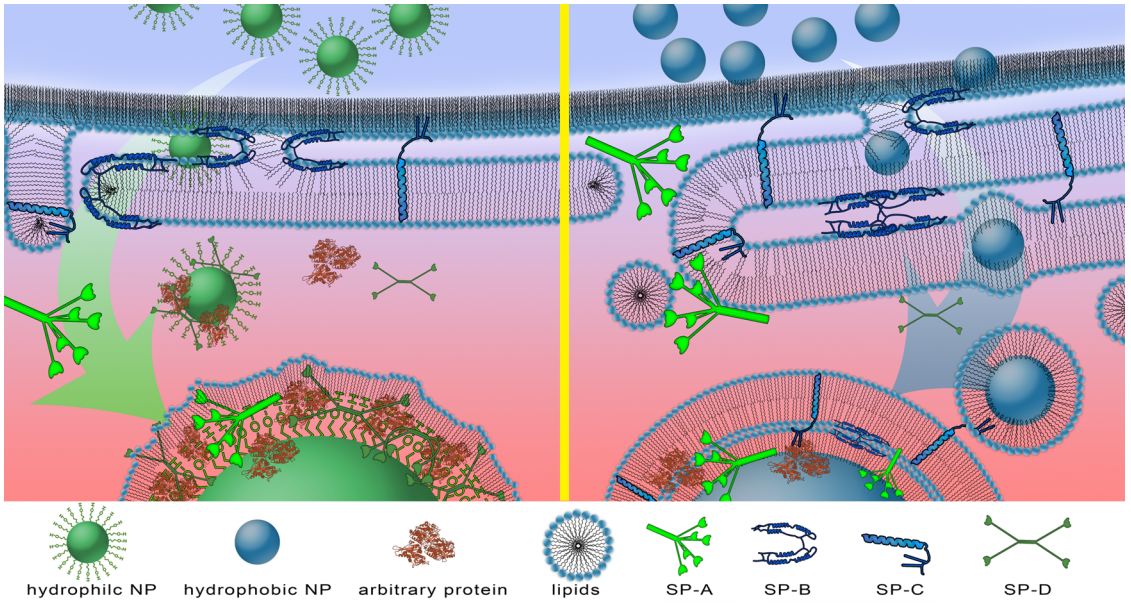

Figure 5. Schematic cartoon of the proposed interaction mechanism of NPs with the pulmonary surfactant layer: Hydrophilic NPs (green) penetrate through the lipid layers.[45] After opsonization by proteins, the lipid binding to the NPs is determined by the lipid−protein interactions. Hydrophobic NPs (blue) can directly interact with the lipid layers and therewith attract mainly proteins that are directly associated with the lipids.

with PL membranes by unspecific hydrophobic binding especially to GPIno, but to a lesser extent than SP-A,[18] which can explain the found lipid adsorption to PEG-NPs. CAMP, which was found mostly on Lipid- and PLGA-NPs, is a antibacterial peptide, readily interacting with membranes and phospholipids. It is part also part of the host defense and a protein that one would expect to find on an lung-intruding particle.[49] The presence of the lipophilic APOA1 in the NP corona in PS is not surprising, as it is commonly found in the plasma corona. SLC34A2 is a phosphate transporter, assumed to be involved in PS genesis. It is membrane bound and highly expressed in the lungs, why it shows tendencies, however, to bind certain NPs cannot be explained. The same applies to MYH3, a rather untypical protein to be found in such a corona with no obvious connection to the PS known so far, although Myosin-18A was identified as a receptor for SP-A.[50] Another interesting protein is deleted in malignant brain tumors 1 protein (DMBT1), whose alternative name is Surfactant pulmonary-associated D-binding protein. In our results, DMBT1 however does not associate with SP-D concentration, but the opposite. It is preferably found on Lipid- before PLGA- and PEG-NPs. DMBT1 is expressed by macrophages and alveolar tissue, partly integrated into membranes, which shows its lipid binding capability and was found to be binding itself to gram-positive and gram-negative bacteria.[51] BPI fold-containing family B member 1 (BPIFB1) and Ficolin 1 + 2 (FCN1, FCN2) are two other proteins within one of the selected thresholds which are capable of binding pathogens and interact with lipids. Table 4 reveals that the same proteins that tend to adsorb to Lipid-NPs, also interact with the PLGA-NPs, although to a lesser extent. PEG-NPs, however do not fit this adsorption pattern, their corona is dominated by the enrichment of SP-D. Of the mentioned 9 proteins, only 4 (APOA1, CAMP, FCN1, and FCN2) are commonly found in plasma. Since serum proteins did not mediate a lipid binding (Figure S4A), one could speculate, that one or more of the remaining proteins are responsible for the observed corona formation.

CONCLUSION AND OUTLOOK

Upon contact of nanoparticles with pulmonary surfactant, a corona is formed which consists of both proteins and lipids. Obviously, such surfactant corona, as it will form around inhaled nanoparticles encountering the alveolar lining fluid first, is clearly different to a plasma corona where the lipid components are missing. Pulmonary surfactant from porcine source (pPS) is from physiological, biochemical and biophysical viewpoints a realistic model for the simulation of the PS layer. Our results show that pPS is also suitable for studying the interactions of PS with nanomaterials. We found a similar lipid composition in the corona of PEG-, PLGA-, and Lipid-NPs, but lower absolute amounts in the corona of the hydrophilic PEG-NPs. The lipid binding to PEG-NPs could not be explained by physicochemical, nor annotated properties of the found proteins, which differed on the NPs, most notably on PEG-NPs. Neither a lipid-binding effect by single proteins, nor interplay of many proteins can be excluded. Among the several hundred proteins identified, there were only a few showing significantly changing abundancies among the three NPs. Those, however, are

mostly capable of binding epitopes of, *e.g.*, surfaces of bacteria and viruses and furthermore to interact with lipids. It is therefore not unlikely that these proteins mediate lipid binding to even rather hydrophilic NPs, such as, *e.g.*, PEGylated ones. Subsequent adsorption of lipids and proteins would equalize the outer surface of coronas formed even around rather different NPs and thus facilitate their interaction with the lung surfactant system (see scheme in Figure 5, left).

A certain limitation of our current study is that we had to rely on magnetic separation. Although we found this to be the most suitable way, future studies might evaluate other possibilities for separating NPs from the native surfactant, making the corona of nonmagnetic NPs also accessible. Depending on the mode of separation, the corona of NPs after contact with PS might not be as readily distinguishable in "hard" and "soft corona", given that there are not only single molecules, but a complex of interacting structures present in the alveolar lining fluid. Since there is always a strong attracting force between the lamellar PS structures and the adsorbed lipid corona, the applied shear forces will determine the amount of vesicular structures attached to the NPs. The binding strength of the hydrophilic NPs toward the lamellar structures of the PS might be depending on the strength of interaction of adsorbed proteins with lipids as illustrated in Figure 5. By evaluating the binding of PS lipid fraction in the presence of single PS proteins, this could be addressed further, although the access to intact isolated surfactant proteins is limited. On the basis of our results, the analysis of the complex fluid could be broken into some more basic analysis due to the fact that the lipid corona seems not to change and consists mostly of just a few different lipid species.

The next logical steps to a further understanding of the PS corona would be a time-dependent resolution of the adsorption behavior, to elucidate the kinetics and prove which biomolecules have an affinity for the surface of NPs. In future, it also needs to be evaluated, how exactly the presence of this lipid−protein corona influences the interaction of nanomaterials with cells. As previous studies from our and other groups showed,[21,52] the corona has an impact on the fate of inhaled NPs when interacting with the biological barriers of the lung. A further point which needs to be addressed is to which extent lipid mono- and bilayer adsorb the NPs. Simple size measurements by DLS are not feasible as the vesicles of PS (as visible in Figure S2) interfere with the NP signal. For this reason, the polydispersity of NPs in the presence of PS is challenging to determine.

Prospective studies will help understanding this very important part of the bionano-interface and will therewith also help to understand the toxicity of incidentally inhaled nanomaterials, as well as to improve the on-purpose delivery of nanomedicines to the deep lung.

MATERIALS AND METHODS

Reagents. Phospholipid standards were purchased from Avanti Polar Lipids (Alabaster, AL), poly(D,L-lactide-*co*-glycolide) (Resomer RG 503 H) from Evonik (Essen, Germany). Magnetic PEG-NP (nanomag-D PEG 5000) and Lipid-NP (fluidMAG-Lipid) were ordered from Micromod (Rostock, Germany) and Chemicell GmbH (Berlin, Germany) respectively, and were used as received. All other reagents and solvents were purchased from Sigma-Aldrich (Munich, Germany).

Broncho Alveolar Lavage Fluid (pBALF). Lungs from freshly slaughtered pigs were chosen in the slaughterhouse by their apparent intact, nondamaged appearance and lavaged immediately with 2−4 L of physiological 0.9% sodium chloride solution under application of gentle massage. Clear pBALF was centrifuged (Rotina 420R + rotor 4794, Hettich) for 5 min at 2000 rpm and 4 °C for cell debris removal and frozen until further purification.

Native Surfactant Preparation (pPS). pPS was purified according to a modified method of Shelley *et al.*[33] as described by Taeusch *et al.*[53] In short, thawed pBALF was centrifuged for 1 h at 31 000 rpm and 4 °C in an Optima L-90K (Beckman Coulter) equipped with a TYPE 70 Ti rotor and the supernatant was discarded. The accumulated pellets were dissolved in a solution of 16% (w/v) sodium bromide and 0.9% sodium chloride, overlaid with a layer of 13% NaBr + 0.9% NaCl and a subsequent layer of 0.9% NaCl. pPS vesicles with a density higher than 1.10 g/cm^3 were separated by density gradient centrifugation (2 h, 28 000 rpm, 4 °C, without brakes) in a swinging bucket rotor (SW 40 Ti, Beckman Coulter). In a final centrifugation step (1 h, 31 000 rpm, 4 °C), the obtained pPS was purified from excess sodium bromide. The white pellets of 8 pig lungs were pooled and stored at −80 °C until usage. Protein (3 mg/mL) and phospholipid concentration (34 mg/mL) were approximated by bicinchoninic acid assay (Sigma-Aldrich, USA) and phosphorus assay[54] respectively.

Preparation of Magnetic PLGA-Nanoparticles. Magnetic PLGA-NPs were prepared by an emulsification-evaporation method.[55] Oleic acid-coated primary magnetite nanoparticles with diameters of ∼10 nm were coprecipitated as described elsewhere.[56] Briefly, poly(D,L-lactide-*co*-glycolide) and magnetite primary nanoparticles were dissolved in chloroform and mixed with a water phase containing 2.5% poly(vinyl alcohol). After tip sonication (Digital Sonifier, Branson; conditions: 1 min, 30% amplitude, on ice) the volume was expanded by addition of water and the chloroform was evaporated overnight. Magnetic PLGA-NPs were purified by separation in a magnetic separator (Merck Millipore, USA) and filtered through a 0.45 μm cellulose acetate membrane to remove primary particle agglomerates. Particle mass concentration was determined gravimetrically.

Particle Characterization. All used particles were characterized by Dynamic Light Scattering (Zetasizer Nano ZSP; Malvern Instruments, USA), Nanoparticle Tracking Analysis (Nanosight LM10; Malvern Instruments), Transmission (JEM 2011; Jeol, Japan) and Scanning Electron Microscopy (EVO HD 15; Zeiss, Germany). All particles used were in the same size- and number-concentration range, with a negative zetapotential; the results of the characterization can be found in the Supporting Information (see Table S2, Figure S6).

Incubation and Separation of NPs. pPS was diluted in tris-buffered saline (TBS = 150 mM NaCl, 5 mM Tris, pH 7.4) to meet a ratio of 1:2 (μg NPs to μg proteins in pPS). Before the addition, the NP dispersions were vortexed and sonicated briefly in an ultrasonic bath. The incubation took place at 37 °C and 400 rpm shaking in order to prevent pelleting of surfactant. An incubation

time of 1 h was regarded as sufficient for reaching equilibrium, as previous studies showed a very fast corona formation within minutes.[5] NPs with the adherent protein and lipid corona were separated magnetically and the supernatant was discarded. The pellet was washed three times by redispersion in 1.5 mL TBS and repeated magnetic separation. After the last washing step, the remaining liquid was centrifuged for 5 min at 10 000 rpm and the supernatant discarded. The pellets were frozen at −80 °C until further analysis.

Lipid Extraction. The frozen NP-pPS pellets were lyophilized (Christ Alpha 2−4 LSC, Martin Christ GmbH) and four times extracted under agitation and sonication with a mixture of IPA: Hexane:Ammonium formate 1% 50:40:10, and once with chloroform:methanol 2:1. Exhaustive extraction was controlled by thin layer chromatography. The solvent was evaporated (Concentrator Plus, Eppendorf) and the samples dissolved in IPA:Hexane:Ammonium formate 1% 50:40:10. Blank particles (*i.e.*, w/o pPS) were extracted as control. Cholesterol was subsequently determined by enzymatic reaction (Amplex Red Cholesterol Assay Kit, Thermo Fisher Scientific).

Normal-Phase Phospholipid Separation. Phospholipids were analyzed after normal phase liquid chromatography as recommended by the LIPID MAPS consortium.[57] Briefly, 10 μL of the organic extract were injected in an LC-System consisting of Accela Autosampler, Accela PDA and Accela 1250 pump (Thermo Fisher Scientific, San Jose, CA), equipped with a 150 × 2.1 mm column (Triart Hilic, YMC, Japan) at 40 °C with a constant flow of 250 μL/min. PL were eluted using a gradient of isopropanol/hexane (60/40 + 0.1% formic acid = solvent A) and isopropanol/hexane/1% ammonium formate buffer (50/40/10 + 0.1% formic acid = solvent B). The starting conditions were 15% solvent B, after 3 min increase to 90% solvent B at 9 min, 100% solvent B at 11 min and a decrease to 90% solvent B again. Afterward, solvent B concentration was decreased to 15% over 1 min and re-equilibrated for five min. These conditions allowed the elution of the lipid classes phosphatidylcholine (GPChol), -glycerol (GPGlyc), -ethanolamine (GPEth), -serine (GPSer), -inositol (GPIno) and sphingomyelins (SM) and furthermore lysophosphatidylcholine (L-GPChol) as discrete peaks.

Electrospray Mass Spectrometry of Phospholipids. From LC, samples were directly infused into a triple quadrupole mass spectrometer (TSQ Quantum Access Max, Thermo Fisher Scientific, San Jose, CA), equipped with an electrospray ionization source (HESI-II). Ionization conditions: spray voltage 3500 V; vaporizer temperature 250 °C; sheath gas pressure 20 au; ion sweep gas pressure 0 au; aux gas pressure 35 au; capillary temperature 270 °C; tube lens offset 101 au; skimmer offset 10 au; collision gas pressure 1.3 mTorr. During method development, the PL peaks were scanned for the individual masses as follows: GPChol, SM, and L-GPChol: precursor +184 *m/z*, CE 30; GPGlyc: NL + 172 *m/z*, CE 13; GPEth: NL + 141 *m/z*, CE 18; GPIno: precursor −241 *m/z*, CE 46; GPSer: NL −87 *m/z*, CE 28. To increase scan time and therewith signal strength, the found ions were monitored in SIM. A total of 277 distinct masses were measured in each run. Each PL species was quantified against an external standard curve of the respective PL class (except for SM, which was compared to the GPChol standard). Xcalibur (Thermo Fisher Scientific, Version 2.2) was used for data acquisition, MzMine (Version 2.10) for data processing.[58] The method was validated for its linearity, limit of detection, limit of quantification, intra- and interday comparison for each individual phospholipid class. Because of the immense differences in concentration between GPChol and the other PL classes, all samples were analyzed at two different concentrations to achieve results in the linear range for all classes.

Label-Free Shotgun Analysis. Isolated nanoparticle-surfactant complexes were suspended in 7 M urea, 2 M thiourea and 2% of CHAPS (all components purchased from Roth) to elute NPs bound proteins. Protein digestion, nanoscale reversed phase liquid chromatography and label-free quantitative proteomic analyses of protein corona components by mass spectrometry using ion-mobility enhanced data-independent acquisition were performed as described in detail previously.[5,39] Relative total amounts—expressed as ppm (parts per million) of total protein—were automatically calculated within each sample based on the TOP3 quantification approach in the ISOQuant software as previously described.[20]

Protein Annotation. Because of the unsatisfactory annotations of porcine proteins in existing databases, all porcine proteins were blasted against the human Swiss-Prot database and the homologue human protein chosen based on E-value and Score. Proteins were annotated with STRAP 1.5.[59] Gravy Score was calculated according to Kyte-Doolittle.

Statistical Tests. For the detection of significantly different data we applied the moderated *t*-test,[60] also known as limma. We used the limma package[61] available from the Bioconductor software project,[62] which provides a free implementation of this test for the R computing environment.[63] Although the moderated *t*-test was originally intended for the analysis of gene expression data arising for example from microarray analyses, its use is not restricted to such data.[64] The moderated *t*-test is comparable to Student's *t*-test in that both methods employ the means to compare the data of both groups for a specified protein and, thus, to estimate the protein's significance in the current comparison. The crucial difference between the two approaches concerns the calculation of variance. Student's *t*-test computes the variance of a protein only based on the data of that protein. The moderated *t*-test uses information from all proteins to calculate the variance by fitting a linear model and employing the empirical Bayes approach.[60] Using this method we obtained a *p*-value for each protein and each comparison. To control the false discovery rate we adjusted the *p*-values in each comparison according to the Benjamini−Hochberg procedure.[65] Finally, only proteins and lipids with adjusted *p*-values less than 0.05 were reported as significantly different.

Conflict of Interest: The authors declare no competing financial interest.

Acknowledgment. We thank Dr. Christian Cavelius (Leibniz Institute for New Materials) for providing primary magnetite NPs and the local slaughterhouse Faerber, Zweibruecken for giving access to their facilities and animal tissue. Chiara De Rossi is thanked for assisting with the LC−MS analysis and proofreading the manuscript. Jesús Pérez-Gil acknowledges funding from Spanish Ministry of Economy (BIO2012-30733) and the Regional Government of Madrid (P2013/MIT2807). Stefan Tenzer and Wiebke Storck were supported by Stiftung Rheinland-Pfalz (NANOSCH) and the DFG (SFB 1080).

Supporting Information Available: The Supporting Information is available free of charge on the ACS Publications website at DOI: 10.1021/acsnano.5b04215.

Scheme of pPS preparation; Dynamic light scattering of pPS membranes; Comparison of separation methods; Most abundant lipid species in pPS and the corona of NPs; Adsorption of Alveofact to NPs; Comparison of protein adsorption by means of MW, IEP, and Gravy Score; Characterization of NPs. (PDF)

List of all proteins and lipids that were determined in pPS and in the corona of NPs. (XLSX)

REFERENCES AND NOTES

1. Nel, A. E.; Madler, L.; Velegol, D.; Xia, T.; Hoek, E. M.; Somasundaran, P.; Klaessig, F.; Castranova, V.; Thompson, M. Understanding Biophysicochemical Interactions at the Nano-Bio Interface. *Nat. Mater.* **2009**, *8*, 543–557.
2. Walczyk, D.; Bombelli, F. B.; Monopoli, M. P.; Lynch, I.; Dawson, K. A. What the Cell "Sees" in Bionanoscience. *J. Am. Chem. Soc.* **2010**, *132*, 5761–5768.
3. Duncan, R.; Gaspar, R. Nanomedicine(s) under the Microscope. *Mol. Pharmaceutics* **2011**, *8*, 2101–2141.
4. Walkey, C. D.; Chan, W. C. Understanding and Controlling the Interaction of Nanomaterials with Proteins in a Physiological Environment. *Chem. Soc. Rev.* **2012**, *41*, 2780–2799.
5. Tenzer, S.; Docter, D.; Kuharev, J.; Musyanovych, A.; Fetz, V.; Hecht, R.; Schlenk, F.; Fischer, D.; Kiouptsi, K.; Reinhardt, C.; *et al.* Rapid Formation of Plasma Protein Corona Critically

Affects Nanoparticle Pathophysiology. *Nat. Nanotechnol.* **2013**, *8*, 772–781.
6. Lynch, I.; Cedervall, T.; Lundqvist, M.; Cabaleiro-Lago, C.; Linse, S.; Dawson, K. A. The Nanoparticle-Protein Complex as a Biological Entity; a Complex Fluids and Surface Science Challenge for the 21st Century. *Adv. Colloid Interface Sci.* **2007**, *134*−*135*, 167–174.
7. Monopoli, M. P.; Walczyk, D.; Campbell, A.; Elia, G.; Lynch, I.; Bombelli, F. B.; Dawson, K. A. Physical-Chemical Aspects of Protein Corona: Relevance to *in Vitro* and *in Vivo* Biological Impacts of Nanoparticles. *J. Am. Chem. Soc.* **2011**, *133*, 2525–2534.
8. Walkey, C. D.; Olsen, J. B.; Song, F.; Liu, R.; Guo, H.; Olsen, D. W.; Cohen, Y.; Emili, A.; Chan, W. C. Protein Corona Fingerprinting Predicts the Cellular Interaction of Gold and Silver Nanoparticles. *ACS Nano* **2014**, *8*, 2439–2455.
9. Behzadi, S.; Serpooshan, V.; Sakhtianchi, R.; Muller, B.; Landfester, K.; Crespy, D.; Mahmoudi, M. Protein Corona Change the Drug Release Profile of Nanocarriers: The "Overlooked" Factor at the Nanobio Interface. *Colloids Surf., B* **2014**, *123*, 143–149.
10. Lesniak, A.; Fenaroli, F.; Monopoli, M. P.; Aberg, C.; Dawson, K. A.; Salvati, A. Effects of the Presence or Absence of a Protein Corona on Silica Nanoparticle Uptake and Impact on Cells. *ACS Nano* **2012**, *6*, 5845–5857.
11. Ge, C.; Tian, J.; Zhao, Y.; Chen, C.; Zhou, R.; Chai, Z. Towards Understanding of Nanoparticle-Protein Corona. *Arch. Toxicol.* **2015**, *89*, 519.
12. Pino, P. d.; Pelaz, B.; Zhang, Q.; Maffre, P.; Nienhaus, G. U.; Parak, W. J. Protein Corona Formation around Nanoparticles − from the Past to the Future. *Mater. Horiz.* **2014**, *1*, 301.
13. Schleh, C.; Kreyling, W. G.; Lehr, C. M. Pulmonary Surfactant Is Indispensable in Order to Simulate the *in Vivo* Situation. *Part. Fibre Toxicol.* **2013**, *10*, 6.
14. Kumar, A.; Forbes, B.; Mudway, I.; Bicer, E. M.; Dailey, L. A. What Are the Biological and Therapeutic Implications of Biomolecule Corona Formation on the Surface of Inhaled Nanomedicines? *Nanomedicine* **2015**, *10*, 343–345.
15. Casals, C.; Canadas, O. Role of Lipid Ordered/Disordered Phase Coexistence in Pulmonary Surfactant Function. *Biochim. Biophys. Acta, Biomembr.* **2012**, *1818*, 2550–2562.
16. Bernardino de la Serna, J.; Oradd, G.; Bagatolli, L. A.; Simonsen, A. C.; Marsh, D.; Lindblom, G.; Perez-Gil, J. Segregated Phases in Pulmonary Surfactant Membranes Do Not Show Coexistence of Lipid Populations with Differentiated Dynamic Properties. *Biophys. J.* **2009**, *97*, 1381–1389.
17. Pérez-Gil, J. Structure of Pulmonary Surfactant Membranes and Films: The Role of Proteins and Lipid-Protein Interactions. *Biochim. Biophys. Acta, Biomembr.* **2008**, *1778*, 1676–1695.
18. Crouch, E.; Wright, J. R. Surfactant Proteins A and D and Pulmonary Host Defense. *Annu. Rev. Physiol.* **2001**, *63*, 521–554.
19. Parra, E.; Pérez-Gil, J. Composition, Structure and Mechanical Properties Define Performance of Pulmonary Surfactant Membranes and Films. *Chem. Phys. Lipids* **2014**, *185*, 153.
20. Tenzer, S.; Docter, D.; Rosfa, S.; Wlodarski, A.; Kuharev, J.; Rekik, A.; Knauer, S. K.; Bantz, C.; Nawroth, T.; Bier, C.; *et al.* Nanoparticle Size Is a Critical Physicochemical Determinant of the Human Blood Plasma Corona: A Comprehensive Quantitative Proteomic Analysis. *ACS Nano* **2011**, *5*, 7155–7167.
21. Ruge, C. A.; Schaefer, U. F.; Herrmann, J.; Kirch, J.; Canadas, O.; Echaide, M.; Pérez-Gil, J.; Casals, C.; Muller, R.; Lehr, C. M. The Interplay of Lung Surfactant Proteins and Lipids Assimilates the Macrophage Clearance of Nanoparticles. *PLoS One* **2012**, *7*, e40775.
22. Kapralov, A. A.; Feng, W. H.; Amoscato, A. A.; Yanamala, N.; Balasubramanian, K.; Winnica, D. E.; Kisin, E. R.; Kotchey, G. P.; Gou, P.; Sparvero, L. J.; *et al.* Adsorption of Surfactant Lipids by Single-Walled Carbon Nanotubes in Mouse Lung Upon Pharyngeal Aspiration. *ACS Nano* **2012**, *6*, 4147–4156.
23. Konduru, N. V.; Tyurina, Y. Y.; Feng, W.; Basova, L. V.; Belikova, N. A.; Bayir, H.; Clark, K.; Rubin, M.; Stolz, D.; Vallhov, H.; *et al.* Phosphatidylserine Targets Single-Walled Carbon Nanotubes to Professional Phagocytes *in Vitro* and *in Vivo*. *PLoS One* **2009**, *4*, e4398.
24. Tyurina, Y. Y.; Kisin, E. R.; Murray, A.; Tyurin, V. A.; Kapralova, V. I.; Sparvero, L. J.; Amoscato, A. A.; Samhan-Arias, A. K.; Swedin, L.; Lahesmaa, R.; *et al.* Global Phospholipidomics Analysis Reveals Selective Pulmonary Peroxidation Profiles Upon Inhalation of Single-Walled Carbon Nanotubes. *ACS Nano* **2011**, *5*, 7342–7353.
25. Sachan, A. K.; Harishchandra, R. K.; Bantz, C.; Maskos, M.; Reichelt, R.; Galla, H. J. High-Resolution Investigation of Nanoparticle Interaction with a Model Pulmonary Surfactant Monolayer. *ACS Nano* **2012**, *6*, 1677–1687.
26. Sachan, A. K.; Galla, H. J. Understanding the Mutual Impact of Interaction between Hydrophobic Nanoparticles and Pulmonary Surfactant Monolayer. *Small* **2014**, *10*, 1069–1075.
27. Landsiedel, R.; Sauer, U. G.; Ma-Hock, L.; Schnekenburger, J.; Wiemann, M. Pulmonary Toxicity of Nanomaterials: A Critical Comparison of Published *in Vitro* Assays and *in Vivo* Inhalation or Instillation Studies. *Nanomedicine (London, U. K.)* **2014**, *9*, 2557–2585.
28. Jones, M. C.; Jones, S. A.; Riffo-Vasquez, Y.; Spina, D.; Hoffman, E.; Morgan, A.; Patel, A.; Page, C.; Forbes, B.; Dailey, L. A. Quantitative Assessment of Nanoparticle Surface Hydrophobicity and Its Influence on Pulmonary Biocompatibility. *J. Controlled Release* **2014**, *183*, 94–104.
29. Fox, G. F.; Sothinathan, U. The Choice of Surfactant for Treatment of Respiratory Distress Syndrome in Preterm Infants: A Review of the Evidence. *Infant* **2005**, *1*, 8–12.
30. Pohlmann, G.; Iwatschenko, P.; Koch, W.; Windt, H.; Rast, M.; de Abreu, M. G.; Taut, F. J. H.; De Muynck, C. A Novel Continuous Powder Aerosolizer (CPA) for Inhalative Administration of Highly Concentrated Recombinant Surfactant Protein-C (rSP-C) Surfactant to Preterm Neonates. *J. Aerosol Med. Pulm. Drug Delivery* **2013**, *26*, 370–379.
31. Beck-Broichsitter, M.; Ruppert, C.; Schmehl, T.; Gunther, A.; Seeger, W. Biophysical Inhibition of Synthetic Vs. Naturally-Derived Pulmonary Surfactant Preparations by Polymeric Nanoparticles. *Biochim. Biophys. Acta, Biomembr.* **2014**, *1838*, 474–481.
32. Blanco, O.; Cruz, A.; Ospina, O. L.; Lopez-Rodriguez, E.; Vazquez, L.; Pérez-Gil, J. Interfacial Behavior and Structural Properties of a Clinical Lung Surfactant from Porcine Source. *Biochim. Biophys. Acta, Biomembr.* **2012**, *1818*, 2756–2766.
33. Shelley, S. A.; Paciga, J. E.; Balis, J. U. Purification of Surfactant from Lung Washings and Washings Contaminated with Blood Constituents. *Lipids* **1977**, *12*, 505–510.
34. Bernhard, W.; Mottaghian, J.; Gebert, A.; Rau, G. A.; von Der, H. H.; Poets, C. F. Commercial *Versus* Native Surfactants. Surface Activity, Molecular Components, and the Effect of Calcium. *Am. J. Respir. Crit. Care Med.* **2000**, *162*, 1524–1533.
35. Casals, C. Role of Surfactant Protein A (Sp-A)/Lipid Interactions for Sp-A Functions in the Lung. *Fetal Pediatr. Pathol.* **2001**, *20*, 249–268.
36. Ogasawara, Y.; Kuroki, Y.; Akino, T. Pulmonary Surfactant Protein D Specifically Binds to Phosphatidylinositol. *J. Biol. Chem.* **1992**, *267*, 21244–21249.
37. Rodríguez Patino, J. M.; Niño, M. R. R. Protein Adsorption and Protein-Lipid Interactions at the Air-Aqueous Solution Interface. *Colloids Surf., A* **1995**, *103*, 91–103.
38. Monopoli, M. P.; Pitek, A. S.; Lynch, I.; Dawson, K. A. Formation and Characterization of the Nanoparticle-Protein Corona. *Methods Mol. Biol.* **2013**, *1025*, 137–155.
39. Docter, D.; Distler, U.; Storck, W.; Kuharev, J.; Wunsch, D.; Hahlbrock, A.; Knauer, S. K.; Tenzer, S.; Stauber, R. H. Quantitative Profiling of the Protein Coronas That Form around Nanoparticles. *Nat. Protoc.* **2014**, *9*, 2030–2044.
40. Monopoli, M. P.; Wan, S. H. A.; Bombelli, F. B.; Mahon, E.; Dawson, K. A. Comparisons of Nanoparticle Protein Corona Complexes Isolated with Different Methods. *Nano LIFE* **2013**, *03*, 1343004.

41. Bernardino de la Serna, J.; Perez-Gil, J.; Simonsen, A. C.; Bagatolli, L. A. Cholesterol Rules: Direct Observation of the Coexistence of Two Fluid Phases in Native Pulmonary Surfactant Membranes at Physiological Temperatures. *J. Biol. Chem.* **2004**, *279*, 40715–40722.
42. Bernhard, W.; Haagsman, H. P.; Tschernig, T.; Poets, C. F.; Postle, A. D.; van Eijk, M. E.; von der Hardt, H. Conductive Airway Surfactant: Surface-Tension Function, Biochemical Composition, and Possible Alveolar Origin. *Am. J. Respir. Cell Mol. Biol.* **1997**, *17*, 41–50.
43. Hu, G.; Jiao, B.; Shi, X.; Valle, R. P.; Fan, Q.; Zuo, Y. Y. Physicochemical Properties of Nanoparticles Regulate Translocation across Pulmonary Surfactant Monolayer and Formation of Lipoprotein Corona. *ACS Nano* **2013**, *7*, 10525–10533.
44. Grek, C. L.; Newton, D. A.; Spyropoulos, D. D.; Baatz, J. E. Hypoxia Up-Regulates Expression of Hemoglobin in Alveolar Epithelial Cells. *Am. J. Respir. Cell Mol. Biol.* **2011**, *44*, 439–447.
45. Newton, D. A.; Rao, K. M.; Dluhy, R. A.; Baatz, J. E. Hemoglobin Is Expressed by Alveolar Epithelial Cells. *J. Biol. Chem.* **2006**, *281*, 5668–5676.
46. Olmeda, B.; Umstead, T. M.; Silveyra, P.; Pascual, A.; Lopez-Barneo, J.; Phelps, D. S.; Floros, J.; Perez-Gil, J. Effect of Hypoxia on Lung Gene Expression and Proteomic Profile: Insights into the Pulmonary Surfactant Response. *J. Proteomics* **2014**, *101*, 179–191.
47. Mason, R. J.; Voelker, D. R. Regulatory Mechanisms of Surfactant Secretion. *Biochim. Biophys. Acta, Mol. Basis Dis.* **1998**, *1408*, 226–240.
48. Klausner, R. D.; Kumar, N.; Weinstein, J. N.; Blumenthal, R.; Flavin, M. Interaction of Tubulin with Phospholipid Vesicles. I. Association with Vesicles at the Phase Transition. *J. Biol. Chem.* **1981**, *256*, 5879–5885.
49. Bals, R.; Wang, X.; Zasloff, M.; Wilson, J. M. The Peptide Antibiotic LL-37/hCAP-18 Is Expressed in Epithelia of the Human Lung Where It Has Broad Antimicrobial Activity at the Airway Surface. *Proc. Natl. Acad. Sci. U. S. A.* **1998**, *95*, 9541–9546.
50. Yang, C. H.; Szeliga, J.; Jordan, J.; Faske, S.; Sever-Chroneos, Z.; Dorsett, B.; Christian, R. E.; Settlage, R. E.; Shabanowitz, J.; Hunt, D. F.; *et al.* Identification of the Surfactant Protein A Receptor 210 as the Unconventional Myosin 18A. *J. Biol. Chem.* **2005**, *280*, 34447–34457.
51. Madsen, J.; Tornoe, I.; Nielsen, O.; Lausen, M.; Krebs, I.; Mollenhauer, J.; Kollender, G.; Poustka, A.; Skjodt, K.; Holmskov, U. Crp-Ductin, the Mouse Homologue of GP-340/Deleted in Malignant Brain Tumors 1 (DMBT1), Binds Gram-Positive and Gram-Negative Bacteria and Interacts with Lung Surfactant Protein D. *Eur. J. Immunol.* **2003**, *33*, 2327–2336.
52. Thorley, A. J.; Ruenraroengsak, P.; Potter, T. E.; Tetley, T. D. Critical Determinants of Uptake and Translocation of Nanoparticles by the Human Pulmonary Alveolar Epithelium. *ACS Nano* **2014**, *8*, 11778–11789.
53. Taeusch, H. W.; Bernardino de la Serna, J.; Perez-Gil, J.; Alonso, C.; Zasadzinski, J. A. Inactivation of Pulmonary Surfactant Due to Serum-Inhibited Adsorption and Reversal by Hydrophilic Polymers: Experimental. *Biophys. J.* **2005**, *89*, 1769–1779.
54. Barenholz, Y.; Amselem, S. Quality Control Assays in the Development and Clinical Use of Liposome-Based Formulations. In *Liposome Technology*, 2nd ed.; Gregoriadis, G., Ed.; CRC Press: Boca Raton, FL., 1993; Vol. I, pp 527−616.
55. Astete, C. E.; Kumar, C. S. S. R.; Sabliov, C. M. Size Control of Poly(D,L-Lactide-*Co*-Glycolide) and Poly(D,L-Lactide-*Co*-Glycolide)-Magnetite Nanoparticles Synthesized by Emulsion Evaporation Technique. *Colloids Surf., A* **2007**, *299*, 209–216.
56. Laurent, S.; Forge, D.; Port, M.; Roch, A.; Robic, C.; Vander Elst, L.; Muller, R. N. Magnetic Iron Oxide Nanoparticles: Synthesis, Stabilization, Vectorization, Physicochemical Characterizations, and Biological Applications. *Chem. Rev.* **2008**, *108*, 2064–2110.
57. Fahy, E.; Sud, M.; Cotter, D.; Subramaniam, S. Lipid Maps Online Tools for Lipid Research. *Nucleic Acids Res.* **2007**, *35*, W606–612.
58. Pluskal, T.; Castillo, S.; Villar-Briones, A.; Oresic, M. Mzmine 2: Modular Framework for Processing, Visualizing, and Analyzing Mass Spectrometry-Based Molecular Profile Data. *BMC Bioinf.* **2010**, *11*, 395.
59. Bhatia, V. N.; Perlman, D. H.; Costello, C. E.; McComb, M. E. Software Tool for Researching Annotations of Proteins: Open-Source Protein Annotation Software with Data Visualization. *Anal. Chem.* **2009**, *81*, 9819–9823.
60. Smyth, G. K. Linear Models and Empirical Bayes Methods for Assessing Differential Expression in Microarray Experiments. *Stat. Appl. Genet. Mol. Biol.* **2004**, *3*, 1.
61. Ritchie, M. E.; Phipson, B.; Wu, D.; Hu, Y.; Law, C. W.; Shi, W.; Smyth, G. K. Limma Powers Differential Expression Analyses for RNA-Sequencing and Microarray Studies. *Nucleic Acids Res.* **2015**, *43*, e47.
62. Gentleman, R. C.; Carey, V. J.; Bates, D. M.; Bolstad, B.; Dettling, M.; Dudoit, S.; Ellis, B.; Gautier, L.; Ge, Y.; Gentry, J.; *et al.* Bioconductor: Open Software Development for Computational Biology and Bioinformatics. *Genome Biol.* **2004**, *5*, R80.
63. R Core Team *R: A Language and Environment for Statistical Computing*; R Foundation for Statistical Computing: Vienna, Austria, 2014.
64. Kammers, K.; Cole, R. N.; Tiengwe, C.; Ruczinski, I. Detecting Significant Changes in Protein Abundance. *EuPa Open Proteomics* **2015**, *7*, 11–19.
65. Benjamini, Y.; Hochberg, Y. Controlling the False Discovery Rate - a Practical and Powerful Approach to Multiple Testing. *J. R. Stat. Soc. Ser. B. (Stat. Method.)* **1995**, *57*, 289–300.